ACS APPLIED MATERIALS & INTERFACES

Research Article

www.acsami.org

Magnetorheological Elastomer Films with Tunable Wetting and Adhesion Properties

Sanghee Lee, Changyong Yim, Wuseok Kim, and Sangmin Jeon*

Department of Chemical Engineering, Pohang University of Science and Technology (POSTECH), 77 Cheongam-Ro, Nam-Gu, Pohang, Gyeongbuk, Republic of Korea

Supporting Information

ABSTRACT: We fabricated magnetorheological elastomer (MRE) films consisting of polydimethylsiloxane and various concentrations of fluorinated carbonyl iron particles. The application of a magnetic field to the MRE film induced changes in the surface morphology due to the alignment of the iron particles along the magnetic field lines. At low concentrations of iron particles and low magnetic field intensities, needle-like microstructures predominated. These structures formed more mountain-like microstructures as the concentration of iron particles or the magnetic field intensity increased. The surface roughness increased the water contact angle from 100° to 160° and decreased the sliding angle from 180° to 10°. The wettability and adhesion properties changed substantially within a few seconds simply upon application of a magnetic field. Cyclical measurements revealed that the transition was completely reversible.

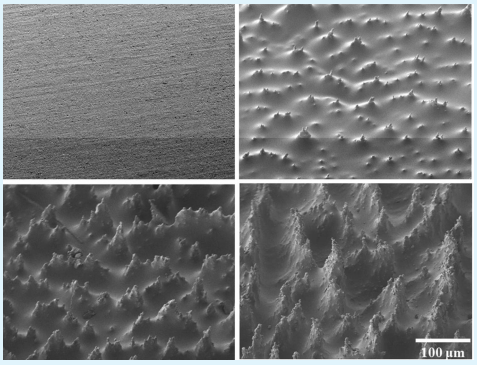

KEYWORDS: *magnetorheological elastomer, superhydrophobic surfaces, contact angle, adhesion, magnetic field*

INTRODUCTION

Inspired by nature's amazing water-repellent surfaces, such as the lotus leaf,[1] water strider's legs,[2] and rose petals,[3] superhydrophobic surfaces with water contact angles exceeding 150° have attracted attention due to their potential uses in a wide range of scientific and industrial applications such as self-cleaning surfaces,[4] oil−water separation,[5,6] filtration membranes,[7,8] antibiofouling coatings,[9] anti-icing coatings,[10] and lossless water transport conduits and containers.[11] Superhydrophobic surfaces are commonly realized by chemically modifying microscopically rough surfaces with low surface energy materials. Although the water contact angle is the most critical parameter that characterizes superhydrophobicity, contact angle hysteresis (the difference between the advancing and receding contact angles) is also an important parameter in applications. Superhydrophobic surfaces that provide a small contact angle hysteresis are suitable for self-cleaning applications due to their low adhesive characteristics. Superhydrophobic surfaces with a large contact angle hysteresis are suitable for lossless water transport applications.[12] Because the application areas of superhydrophobic surfaces demand certain ranges of wettability and adhesion properties, it is important to develop methods for tuning surface properties and expanding their applicability.

Several groups have attempted to alter surface wettability and adhesion properties by applying external stimuli, such as light,[13] temperature,[14] electrical fields,[15] and pH,[16] to trigger a transition in the conformation, polarity, or morphology of the surface material. Relatively few such attempts have used a magnetic field to alter the wettability and adhesion properties. Jiang applied a magnetic field to modulate the adhesive force and transport a liquid drop from one surface to the other. This approach worked only when the water droplet contained magnetic particles.[17,18] Stroeve modulated the water contact angle by inducing a change in the conformation of the magnetic nanopillars on a substrate, but the fabrication of a nanostructured surface was quite complicated, and the water contact angle change did not exceed 20°.[19,20]

In the present study, we fabricated hydrophobic magnetorheological elastomer (MRE) films consisting of a polymeric elastomer and magnetizable particles. Both the wettability and the adhesion properties of the films could be tuned by the application of a magnetic field. The alignment of the magnetizable particles along the magnetic field lines increased the roughness of the MRE surface and affected the water contact angle and sliding angle. The water contact angle could be changed from 100° without a magnetic field to 160° with a magnetic field. The water sliding angle changed from 10° in the presence of a magnetic field to 180° in the absence of a magnetic field. In addition, the morphology change occurred almost immediately and reversibly upon application or withdrawal of the magnetic field. This paper reports the first fabrication of superhydrophobic MRE films with tunable wettability and adhesion properties.

Received: July 13, 2015
Accepted: August 24, 2015
Published: August 24, 2015

DOI: 10.1021/acsami.5b06273
ACS Appl. Mater. Interfaces 2015, 7, 19853−19856

EXPERIMENTAL SECTION

Materials. Carbonyl iron (6−9 μm) and perfluorodecyltriethoxysilane were purchased from Sigma-Aldrich. The carbonyl iron was used as a magnetizable particle source due to its high saturation magnetization (2.1 T). The polydimethylsiloxane (PDMS) precursor and a curing agent (Sylgard 184) were obtained from Dow Corning. Carbonyl iron particles were mixed with PDMS to produce MREs and were used in the subsequent experiment. Disk-shaped 4 mm diameter neodymium permanent magnets with different thicknesses were purchased from Seoul Magnetic (Seoul, Korea), and the remanences of the magnets were 155 mT, 210 mT, and 250 mT for 1, 1.5, and 2 mm thick magnets, respectively.

Preparation of MREs with Various Carbonyl Iron Particle Compositions. The aggregation of carbonyl iron particles in the polymer matrix was suppressed, and their hydrophobicity was increased by chemically modifying the surfaces of the carbonyl iron particles. The carbonyl iron particles were incubated in a 10 mM perfluorodecyltriethoxysilane solution in hexane for 2 h to render their surfaces hydrophobic. The fluorinated carbonyl iron particles were rinsed with hexane and dried at 70 °C. Seven types of MREs were prepared by mixing PDMS with various concentrations of the carbonyl iron particles: MRE10 (10 wt %), MRE20 (20 wt %), MRE30 (30 wt %), MRE40 (40 wt %), MRE50 (50 wt %), MRE60 (60 wt %), and MRE70 (70 wt %). Each MRE film was prepared on a stainless steel substrate using the doctor-blade method, and the resulting film thickness was 150 μm. The MRE surfaces used for the measurements of contact angles and sliding angles were not cured.

Characterization of the MREs. The surface morphologies of the MRE films in the presence of various magnetic field strengths were examined by field-emission scanning electron microscopy (FE-SEM, JEOL). Because the morphologies relied on the continuous application of the magnetic field, the MRE films were cured at 60 °C for 4 h to fix their surface morphologies prior to SEM imaging and surface roughness measurement (Alpha-Step IQ, Tencor Instrument). The water contact angle and sliding angle of the MRE films (uncured) were measured using SmartDrop (FEMTOFAB, Korea) with a 5 μL water droplet.

RESULTS AND DISCUSSION

Figure 1 shows SEM images of an MRE70 film prepared under different magnetic field strengths. In the absence of the applied magnetic field, the surface was quite flat, indicating that all carbonyl iron particles were embedded inside the PDMS film. As the applied magnetic field increased to 155 mT, needle-like microstructures appeared due to the alignment of the iron particles along the magnetic field lines. The number of microstructures present was proportional to the density of the magnetic field line, which depended on the strength of the applied magnetic field. Further increases in the magnetic field strength did not increase the number of microstructures present, although the microstructure size did increase. Because the iron particles were embedded in the viscous PDMS matrix, an increase in the magnetic field induced overlap between the needle-like microstructures to produce large mountain-like microstructures. The inset of Figure 1, panel d shows a magnified SEM image of the microstructure identified in the box. The fluorinated iron particles embedded in the PDMS rose to the surface, thereby increasing the surface roughness and the hydrophobicity compared to the corresponding properties of the pure PDMS layer.

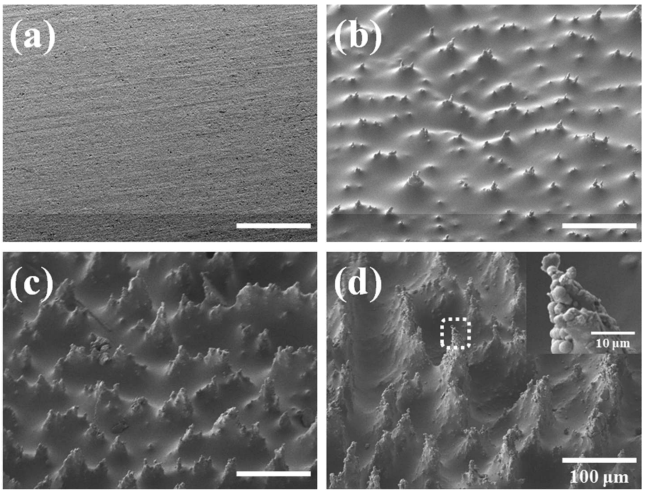

Figure 1. SEM images of MRE70 surfaces under different applied magnetic field strengths: (a) 0 mT, (b) 155 mT, (c) 210 mT, (d) 250 mT. The inset shows a magnified image of the boxed region.

The roughness of each MRE film could be modulated by varying the concentration of iron particles, holding the magnetic field strength constant. Figure 2 shows SEM images of the MRE surfaces prepared at different concentrations of carbonyl iron particles under a 250 mT magnetic field. The low density of iron particles in MRE10 produced a small number of low-profile microstructures that were not very noticeable. As the iron particle concentration increased to 30 wt %, both the number and size of microstructures increased. Further increases in the particle concentration did not increase the number of the microstructures, although the microstructure size did increase due to overlap among the microstructures. The surface roughness (R_a) was measured at five different locations on MRE10, MRE20, MRE30, MRE40, MRE50, and MRE60 and was found to be 93.4 ± 72.6 nm, 158.2 ± 94.8 nm, 259.8 ± 29.3 nm, 498.8 ± 125.0 nm, 575.1 ± 80.2 nm, 1191.9 ± 277.9 nm, respectively. The magnetic field-dependent roughness offers a route to tuning the wettability and adhesion properties of MRE surfaces.

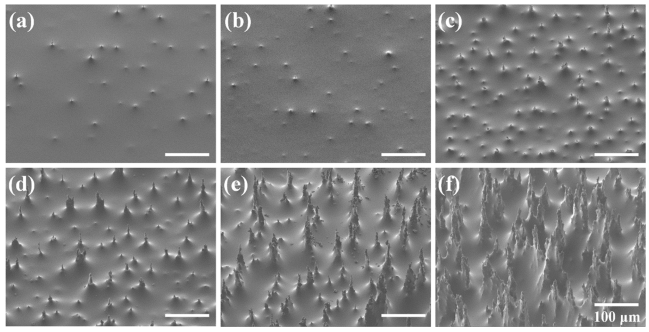

Figure 2. SEM images of MRE surfaces prepared with different concentrations of carbonyl iron particles under a 250 mT magnetic field: (a) MRE10, (b) MRE20, (c) MRE30, (d) MRE40, (e) MRE50, (f) MRE60.

Figure 3 shows optical microscopy images of water droplets on the MRE films prepared with different concentrations of carbonyl iron particles under a 250 mT magnetic field. The water contact angles of MRE10, MRE20, MRE30, MRE40, MRE 50, MRE60, and MRE70 were obtained at five different positions of each MRE surface and were measured to be 101.1 ± 1.1°, 106.4 ± 0.9°, 109.1 ± 0.2°, 123.1 ± 2.1°, 136.6 ± 2.0°, 159.1 ± 2.7°, and 163.0 ± 2.3°, respectively. Note that the water contact angle of PDMS is 102°, similar to that of MRE10, which indicates that the roughness of MRE10 was not sufficient

DOI: 10.1021/acsami.5b06273
ACS Appl. Mater. Interfaces 2015, 7, 19853−19856

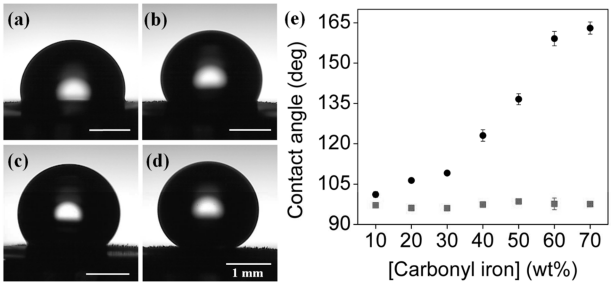

Figure 3. Optical microscopy images of water droplets on the MRE surfaces prepared with different concentrations of carbonyl iron particles: (a) MRE20, (b) MRE40, (c) MRE50, (d) MRE60. The water droplet was 5 μL. (e) Variations in the water contact angle as a function of the concentration of iron particles with a magnetic field of 250 mT (black circle) and without a magnetic field (gray square).

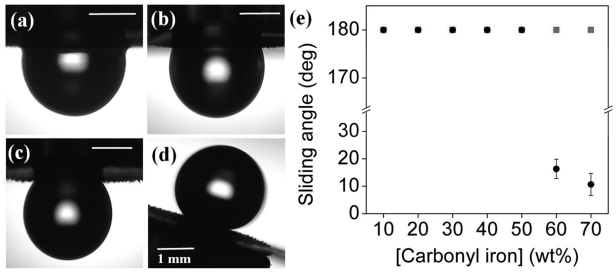

Figure 5. Optical microscopy images of a water droplet on the MRE surfaces prepared with different concentrations of carbonyl iron particles: (a) MRE20, (b) MRE40, (c) MRE50, (d) MRE60. (e) Variations in the sliding angle of a water droplet as a function of the concentration of iron particles with a magnetic field of 250 mT (black circle) and without a magnetic field (gray square).

to affect the surface wettability (see Figure 2a). An increase in the surface roughness increased the water contact angles, and MRE60 exhibited superhydrophobicity, which appears when air trapped between the microstructures hinders direct contact between the water and the surface. The water contact angle on the nanostructured surface was affected by the surface fraction of solid (f_1) and the surface fraction of air (f_2) according to the Cassie and Baxter model:[21]

$$\cos\theta^* = f_1 \cos\theta - f_2 \quad (1)$$

where $f_1 + f_2 = 1$, and θ^* and θ are the apparent water contact angle on a rough surface and a smooth surface of the same material, respectively. Eq 1 indicates that the MRE surface became more hydrophobic as the volume of air trapped among the microstructures increased.

Figure 4, panel a shows optical microscopy images of a water droplet on MRE60 in the presence or absence of a 250 mT magnetic field. The water contact angles of MRE60 were measured to be 159° and 100° in the presence and absence of the magnetic field, respectively, due to changes in the surface roughness. Figure 4, panel b illustrates the transition between the hydrophobic and superhydrophobic surface properties, achieved by alternating the applied magnetic field strength. The transition was found to be reversible under cyclic measurements, and the surface morphology changed within a few seconds. By contrast, conventional methods using UV irradiation require transition times of a few days or are not reversible at all because permanent changes in the surface chemistries are obtained.[22,23]

In addition to the water contact angle, the surface roughness of the MRE films affected the water adhesion properties. Figure 5, panels a–d show optical microscopy images of a water droplet on the MRE20, MRE40, MRE50, and MRE60 films. The advancing (θ_A) and receding (θ_R) contact angles of MRE20, MRE40, MRE 50, and MRE60 were measured to be (θ_A, 114.7°; θ_R, 91.3°), (θ_A, 123.3°; θ_R, 98.3°), (θ_A, 141.5°; θ_R, 106.9°), and (θ_A, 161°; θ_R, 159°), respectively. A water droplet remained adhered to the MRE20, MRE40, and MRE50 films upon 180° inversion of the substrate due to the large water contact angle hysteresis ($\theta_A - \theta_R$), which produced an adhesion force sufficient to hold up the water droplet against the gravitational force.[24] By contrast, the water droplet rolled off the MRE60 surface at a small tilt angle due to the presence of an elastic air layer under the water droplet.[25] The differences between the adhesion properties arose from the different contact areas between the water droplet and the underlying surface. The values of f_1 were calculated using eq 1 and were found to be 0.98, 0.61, 0.37, and 0.089 for MRE20, MRE40, MRE50, and MRE60, respectively, confirming that the water–solid contact area decreased as the concentration of iron particles increased. Figure 5, panel e shows the variations in the sliding angle of a water droplet as a function of the concentration of iron particles under a magnetic field strength of 250 mT. No droplet sliding was observed on the MRE surfaces prepared with a concentration lower than 50 wt %, whereas the sliding angles of MRE60 and MRE70 were 16.3° and 10.6°, respectively. Note that the sliding angles of MRE60 and MRE70, in the absence of a magnetic field, were 180°, and the transition between adhesion and sliding, achieved by alternating the magnetic field, was reversible, as with the water contact angle.

CONCLUSIONS

In summary, we fabricated MRE films consisting of PDMS and carbonyl iron particles, and we investigated the wettability and adhesion properties of the film surfaces under an applied magnetic field. The application of a magnetic field to flat MRE films induced the formation of microstructures due to

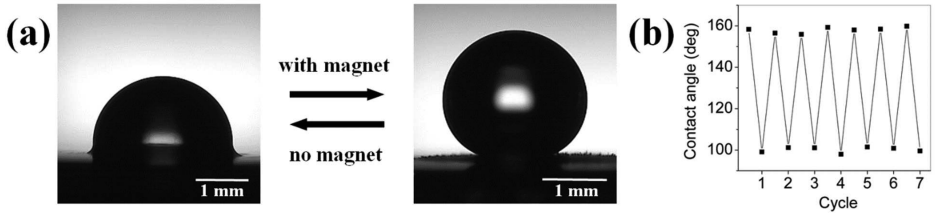

Figure 4. (a) Optical microscopy images of a water droplet on MRE60 in the presence or absence of a 250 mT magnetic field. (b) Reversible switching characteristics of the water contact angle, achieved by alternating the magnetic field strength.

DOI: 10.1021/acsami.5b06273
ACS Appl. Mater. Interfaces 2015, 7, 19853–19856

alignment among the iron particles along the magnetic field lines. Greater changes in the surface roughness were achieved as the concentration of iron particles or the intensity of the applied magnetic field was increased. The changes in the wettability and adhesion properties of the MRE films were completely reversible, and substantial changes in the surface properties were obtained within a few seconds simply by applying a magnetic field. Because the MRE film may be readily applied to any substrate, it may have great potential utility in a wide range of applications including liquid manipulation in microfluidic devices.

■ ASSOCIATED CONTENT

Supporting Information

The Supporting Information is available free of charge on the ACS Publications website at DOI: 10.1021/acsami.5b06273.

Variations in water contact angle under magnetic field (PDF)

■ AUTHOR INFORMATION

Corresponding Author

*E-mail: jeons@postech.ac.kr.

Notes

The authors declare no competing financial interest.

■ ACKNOWLEDGMENTS

This research was supported by Grant No. 15CTAP-C077604-02 funded by the Ministry of Land, Infrastructure, and Transport of Korean government.

■ REFERENCES

(1) Neinhuis, C.; Barthlott, W. Characterization and Distribution of Water-repellent, Self-cleaning Plant Surfaces. *Ann. Bot.* **1997**, *79* (6), 667−677.

(2) Gao, X.; Jiang, L. Biophysics: Water-repellent legs of water striders. *Nature* **2004**, *432* (7013), 36−36.

(3) Feng, L.; Zhang, Y.; Xi, J.; Zhu, Y.; Wang, N.; Xia, F.; Jiang, L. Petal Effect: A Superhydrophobic State with High Adhesive Force. *Langmuir* **2008**, *24* (8), 4114−4119.

(4) Sasmal, A. K.; Mondal, C.; Sinha, A. K.; Gauri, S. S.; Pal, J.; Aditya, T.; Ganguly, M.; Dey, S.; Pal, T. Fabrication of Superhydrophobic Copper Surface on Various Substrates for Roll-off, Self-Cleaning, and Water/Oil Separation. *ACS Appl. Mater. Interfaces* **2014**, *6* (24), 22034−22043.

(5) Zhang, W.; Shi, Z.; Zhang, F.; Liu, X.; Jin, J.; Jiang, L. Superhydrophobic and Superoleophilic PVDF Membranes for Effective Separation of Water-in-Oil Emulsions with High Flux. *Adv. Mater.* **2013**, *25* (14), 2071−2076.

(6) Xue, Z.; Wang, S.; Lin, L.; Chen, L.; Liu, M.; Feng, L.; Jiang, L. A Novel Superhydrophilic and Underwater Superoleophobic Hydrogel-Coated Mesh for Oil/Water Separation. *Adv. Mater.* **2011**, *23* (37), 4270−4273.

(7) Cho, S. J.; Nam, H.; Ryu, H.; Lim, G. A Rubberlike Stretchable Fibrous Membrane with Anti-Wettability and Gas Breathability. *Adv. Funct. Mater.* **2013**, *23* (45), 5577−5584.

(8) Liang, S.; Kang, Y.; Tiraferri, A.; Giannelis, E. P.; Huang, X.; Elimelech, M. Highly Hydrophilic Polyvinylidene Fluoride (PVDF) Ultrafiltration Membranes via Postfabrication Grafting of Surface-Tailored Silica Nanoparticles. *ACS Appl. Mater. Interfaces* **2013**, *5* (14), 6694−6703.

(9) Leslie, D. C.; Waterhouse, A.; Berthet, J. B.; Valentin, T. M.; Watters, A. L.; Jain, A.; Kim, P.; Hatton, B. D.; Nedder, A.; Donovan, K.; Super, E. H.; Howell, C.; Johnson, C. P.; Vu, T. L.; Bolgen, D. E.; Rifai, S.; Hansen, A. R.; Aizenberg, M.; Super, M.; Aizenberg, J.; Ingber, D. E. A bioinspired omniphobic surface coating on medical devices prevents thrombosis and biofouling. *Nat. Biotechnol.* **2014**, *32* (11), 1134−1140.

(10) Lee, M.; Yim, C.; Jeon, S. Communication: Anti-icing characteristics of superhydrophobic surfaces investigated by quartz crystal microresonators. *J. Chem. Phys.* **2015**, *142* (4), 041102.

(11) Mertaniemi, H.; Jokinen, V.; Sainiemi, L.; Franssila, S.; Marmur, A.; Ikkala, O.; Ras, R. H. A. Superhydrophobic Tracks for Low-Friction, Guided Transport of Water Droplets. *Adv. Mater.* **2011**, *23* (26), 2911−2914.

(12) Jin, M.; Feng, X.; Feng, L.; Sun, T.; Zhai, J.; Li, T.; Jiang, L. Superhydrophobic Aligned Polystyrene Nanotube Films with High Adhesive Force. *Adv. Mater.* **2005**, *17* (16), 1977−1981.

(13) Uyama, A.; Yamazoe, S.; Shigematsu, S.; Morimoto, M.; Yokojima, S.; Mayama, H.; Kojima, Y.; Nakamura, S.; Uchida, K. Reversible Photocontrol of Surface Wettability between Hydrophilic and Superhydrophobic Surfaces on an Asymmetric Diarylethene Solid Surface. *Langmuir* **2011**, *27* (10), 6395−6400.

(14) Li, C.; Guo, R.; Jiang, X.; Hu, S.; Li, L.; Cao, X.; Yang, H.; Song, Y.; Ma, Y.; Jiang, L. Reversible Switching of Water-Droplet Mobility on a Superhydrophobic Surface Based on a Phase Transition of a Side-Chain Liquid-Crystal Polymer. *Adv. Mater.* **2009**, *21* (42), 4254−4258.

(15) Lahann, J.; Mitragotri, S.; Tran, T.-N.; Kaido, H.; Sundaram, J.; Choi, I. S.; Hoffer, S.; Somorjai, G. A.; Langer, R. A Reversibly Switching Surface. *Science* **2003**, *299* (5605), 371−374.

(16) Wang, S.; Liu, H.; Liu, D.; Ma, X.; Fang, X.; Jiang, L. Enthalpy-Driven Three-State Switching of a Superhydrophilic/Superhydrophobic Surface. *Angew. Chem., Int. Ed.* **2007**, *46* (21), 3915−3917.

(17) Hong, X.; Gao, X.; Jiang, L. Application of Superhydrophobic Surface with High Adhesive Force in No Lost Transport of Superparamagnetic Microdroplet. *J. Am. Chem. Soc.* **2007**, *129* (6), 1478−1479.

(18) Cheng, Z.; Feng, L.; Jiang, L. Tunable Adhesive Superhydrophobic Surfaces for Superparamagnetic Microdroplets. *Adv. Funct. Mater.* **2008**, *18* (20), 3219−3225.

(19) Fang, J.; Wang, H.; Xue, Y.; Wang, X.; Lin, T. Magnet-Induced Temporary Superhydrophobic Coatings from One-Pot Synthesized Hydrophobic Magnetic Nanoparticles. *ACS Appl. Mater. Interfaces* **2010**, *2* (5), 1449−1455.

(20) Zhou, Q.; Ristenpart, W. D.; Stroeve, P. Magnetically Induced Decrease in Droplet Contact Angle on Nanostructured Surfaces. *Langmuir* **2011**, *27* (19), 11747−11751.

(21) Cassie, A. B. D.; Baxter, S. Wettability of porous surfaces. *Trans. Faraday Soc.* **1944**, *40* (0), 546−551.

(22) Caputo, G.; Cortese, B.; Nobile, C.; Salerno, M.; Cingolani, R.; Gigli, G.; Cozzoli, P. D.; Athanassiou, A. Reversibly Light-Switchable Wettability of Hybrid Organic/Inorganic Surfaces With Dual Micro-/Nanoscale Roughness. *Adv. Funct. Mater.* **2009**, *19* (8), 1149−1157.

(23) Hersey, J. S.; Freedman, J. D.; Grinstaff, M. W. Photoactive electrospun polymeric meshes: spatiotemporally wetting of textured 3-dimensional structures. *J. Mater. Chem. B* **2014**, *2* (20), 2974−2977.

(24) McHale, G.; Shirtcliffe, N. J.; Newton, M. I. Contact-Angle Hysteresis on Super-Hydrophobic Surfaces. *Langmuir* **2004**, *20* (23), 10146−10149.

(25) Huang, X.-J.; Kim, D.-H.; Im, M.; Lee, J.-H.; Yoon, J. B.; Choi, Y.-K. Lock-and-Key" Geometry Effect of Patterned Surfaces: Wettability and Switching of Adhesive Force. *Small* **2009**, *5* (1), 90−94.

DOI: 10.1021/acsami.5b06273
ACS Appl. Mater. Interfaces 2015, 7, 19853−19856